Engineering Fracture Mechanics Vol. 35, No. 1/2/3, pp. 159–170, 1990
Printed in Great Britain.

0013-7944/90 $3.00 + 0.00
Pergamon Press plc.

SIZE EFFECTS IN THE MIXED MODE CRACK PROPAGATION: SOFTENING AND SNAP-BACK ANALYSIS

P. BOCCA,† A. CARPINTERI‡ and S. VALENTE‡

†Istituto Universitario di Architettura di Venezia, 30125 Venezia, Italy; ‡Department of Structural Engineering, Politecnico di Torino, 10129 Torino, Italy

Abstract—Strain softening and localization in concrete are described by means of a cohesive crack model. Whereas for mode I, only untying of the finite element nodes is applied to simulate crack growth, for mixed mode interelement crack propagation topological variation is required at each step. In the case of four point shear testing, the load vs deflection diagrams reveal snap-back instability for large sizes. By increasing the specimen sizes, such instability tends to reproduce the classical LEFM instability, predicted by the Maximum Circumferential Stress Criterion. The fracture toughness parameter of concrete appears to be unique and represented by the mode I fracture energy G_F or the stress-intensity factor K_{IC}, even for mixed mode problems.

1. INTRODUCTION

THE INFLUENCE of shear on the process of cracking of concrete structures is of great practical importance. In the terminology of fracture mechanics, this is called mode II or mixed mode loading.

According to the cohesive crack model, the non-linear crack behaviour can be described by means of cohesive forces in the damage zone, representing the aggregate interlocking and bridging[1–5]. In this way, strain-softening and strain localization are taken into account. The FEM-crack propagation requires a continuous modification of the mesh. Whereas for mode I, only node untying is applied to simulate crack growth, for mixed mode interelement crack propagation a topological variation is performed at each step automatically[6].

The numerical simulation of four point shear specimens of concrete is presented. The load vs loading point deflection curves reveal snap-back instability in some cases, i.e. a softening branch with positive slope. If the loading process were experimentally controlled by the deflection, the loading capacity would undergo a negative jump and a fast and incontrollable crack propagation would occur. On the other hand, the loading process appears stable and the crack propagation slow in the experiments, by controlling crack mouth opening or sliding displacement, which are monotonically increasing functions of the crack length.

The mixed mode brittle fractures (large size) are then interpretable in terms of snap-back instability. Their virtual development can be analysed by the implemented procedure, whereas LEFM describes only the instability condition. On the other hand, the mixed mode ductile fractures (small size) are substantially preceded and obscured by the splitting failure at the specimen centre[7, 8].

The amount of energy dissipated in the localized mixed mode fracture zone results to be approximately equal to the product of mode I fracture energy G_F by total fracture area. Therefore, the introduction of an additional fracture toughness parameter for mixed mode problems, appears unnecessary. The assumption of the "Maximum Circumferential Stress Criterion"[9], for which any crack growth step is produced by a mode I (or opening) mechanism, seems to be confirmed by the experimental results.

2. EXPERIMENTAL PROGRAM

For the four point shear test, twenty-seven (27) concrete specimens were made. The amount of Portland cement was 350 kg/m^3, while the water/cement ratio was about 0.5. The maximum diameter of the alluvial aggregate was $D_{max} = 10$ mm. The compressive strength obtained from six (6) cubic specimens of 16 cm side resulted equal to 33.7 MPa. The specimens were cured for 90 days at 20°C and 65% relative humidity.

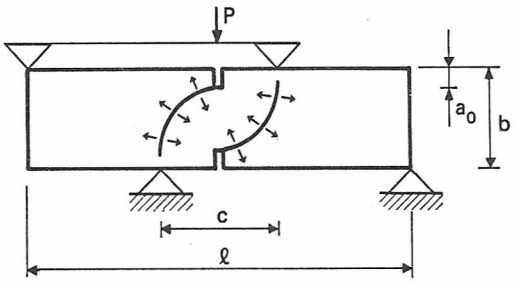

Fig. 1. Four point shear specimen.

The geometrical features of the specimens are the following (Figs 1 and 2): depth $b = 5$, 10, 20 cm; span $l = 4b$; thickness $t = 10$ cm; crack depth $a = 0.2\,b$; and c/b ratio = 0.4; 0.8; 1.2. Specimen geometry, support configuration, average maximum load and mechanical properties are provided in Table 1.

The testing apparatus is shown in Fig. 3. The MTS machine (max. load = 10^4 N) imposed a constant crack mouth sliding displacement rate equal to 2.5×10^{-8} m/s, through the displacement transducer Hottinger Baldwin DD1. Through a similar transducer even the load vs crack mouth opening displacement diagram was recorded, together with the load vs loading point deflection diagram related to the support closer to the center.

In addition, four (4) specimens of sizes $10 \times 10 \times 80$ cm, were tested in three point bending according to the RILEM Recommendation[10]. The mode I fracture energy resulted to be $G_F \approx 100$ N/m.

3. MIXED MODE COHESIVE CRACK AND SNAP-BACK INSTABILITY

The snap-back load–displacement branch may be captured *experimentally* only if the loading process is controlled by a monotonically increasing function of *time*, e.g. the crack mouth opening or sliding displacement. On the other hand, the snap-back load–displacement branch may be captured *numerically* only if the loading process is controlled by a monotonically increasing function of the *crack length*. An example of such functions is provided by the "indirect displacement control scheme"[11]. This technique uses a displacement norm as controlling parameter. On the other hand, as a monotonically increasing function of the crack length, it is possible to use the crack length itself[4, 5]. The same numerical procedure based on discrete cohesive crack modelling, was then extended from mode I to mixed mode crack propagation in [6].

Some dimensionless load–deflection diagrams obtained numerically for a three point bending specimen, with initial crack depth $a_0 = 0.1b$ and ultimate strain $\epsilon_u = 0.87 \times 10^{-4}$, are displayed in Fig. 4, by varying the brittleness number:

$$s_E = \frac{G_F}{\sigma_u b}. \tag{1}$$

Table 1. Specimen geometry, support configuration and mechanical properties

Specimen size	Number of specimens	b	l	t $[m \cdot 10^{-2}]$	a	c/b	P_{max} [dn]	E [MPa]	σ_u [MPa]	G_F [N/m]
A	3	5	20	10	1	0.4	1190	27000	2	100
	3	5	20	10	1	0.8	1222	27000	2	100
	3	5	20	10	1	1.2	1370	27000	2	100
B	3	10	40	10	2	0.4	2027	27000	2	100
	3	10	40	10	2	0.8	1980	27000	2	100
	3	10	40	10	2	1.2	1535	27000	2	100
C	3	20	80	10	4	0.4	3493	27000	2	100
	3	20	80	10	4	0.8	3446	27000	2	100
	3	20	80	10	4	1.2	3700	27000	2	100

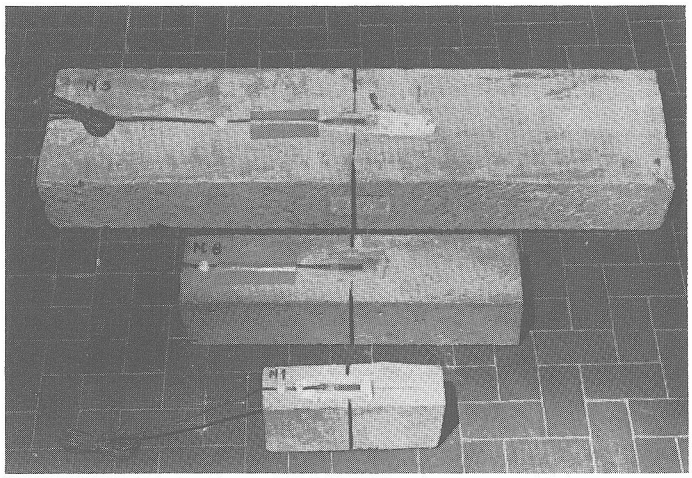

Fig. 2. Different specimen sizes selected for the experimental investigation.

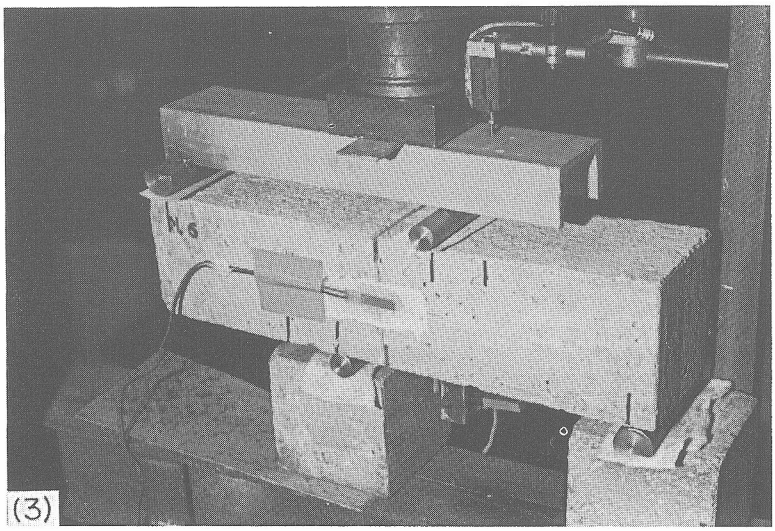

Fig. 3. Testing apparatus.

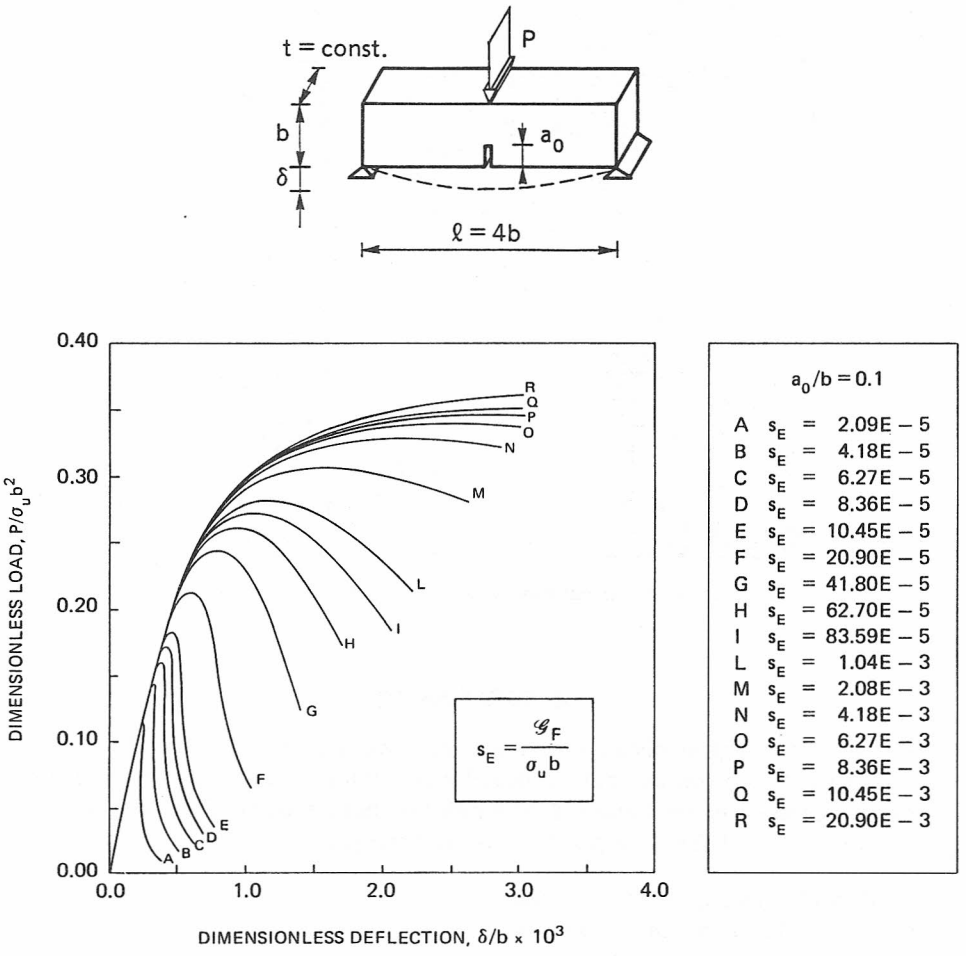

Fig. 4. Size effect on the three point bending behaviour.

The specimen is brittle for low s_E numbers, i.e. for low fracture energies, G_F, high tensile strengths, σ_u, and large sizes, b. For $s_E \lesssim 10.0 \times 10^{-5}$, the p–δ curve presents a softening part with positive slope and a catastrophical event (snap-back) occurs if the loading process is deflection-controlled.

Whereas for mode I, only node untying was applied to simulate crack propagation, for mixed mode interelement crack propagation a continuous modification of the mesh was required. The numerical response of a four point shear specimen (Fig. 5a) is then presented. A finite element rosette was translated and rotated at each non-collinear crack growth step. Figure 5(b) shows two different steps of the crack propagation process. The presence of the cohesive forces is shown by the connections. At the first step the cohesive zone is missing and the load P producing the ultimate tensile stress at the crack tip is computed. Such a value, P, together with the related loading point displacement, δ, gives the first point of the P–δ curve. The fictitious crack tip propagates by a pre-defined length Δa in a direction orthogonal to the maximum circumferential stress[9]. Then, the load P producing the ultimate tensile stress at the up-dated fictitious crack tip and the related deflection δ are computed at each step in order to obtain the subsequent points of the curve.

Some dimensionless load–displacement diagrams obtained numerically for the four point shear specimen are displayed in Fig. 6, by varying the number s_E. Even in this case, the curves reveal a snap-back instability, when $s_E \lesssim 75.0 \times 10^{-5}$.

The mixed mode brittle fractures are interpretable in terms of snap-back instability. Their virtual development may be analysed by the previously presented "fictitious crack length control scheme", whereas LEFM describes only the instability condition.

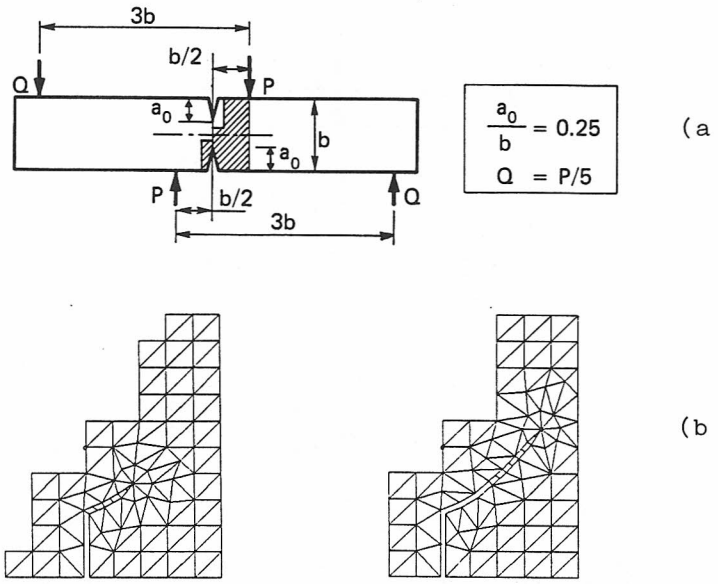

Fig. 5. Subsequent finite element meshes in the analysis of four point shear specimen.

4. DISCUSSION

In the case of the largest distance between the central supports, $c/b = 1.2$ (Fig. 1), flexural failure at the supports is achieved prior to mixed mode crack propagation for each specimen size. In the remaining cases, $c/b = 0.4$ and 0.8, two different failure mechanisms are in competition by varying the size scale b of the four point shear specimen[12]:

(1) mixed mode crack propagation; and
(2) splitting at the center of the specimen.

By increasing the size-scale of a concrete element, the heterogeneity disappears and the influence of the cohesive crack tip forces vanishes, so that the crack propagation is governed only by the linear elastic stress-singularity in the crack tip region[4, 5]. This means that LEFM is a valid crack branching criterion for large concrete structures.

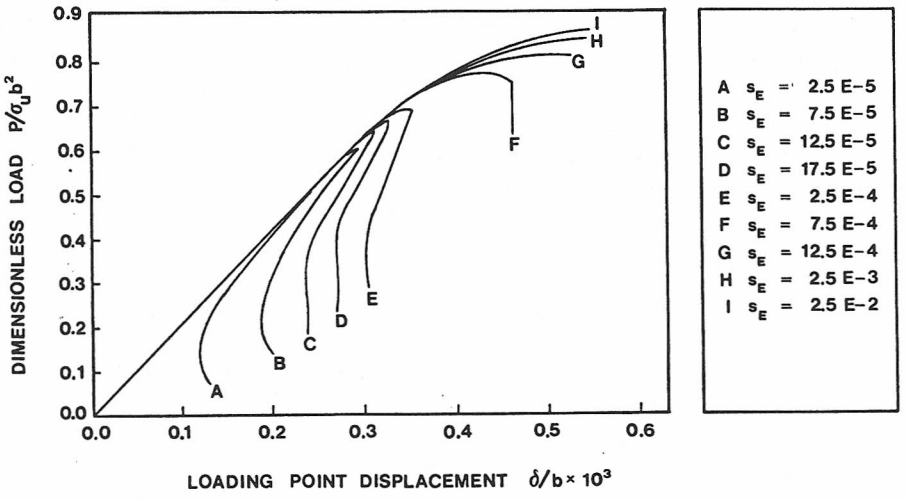

Fig. 6. Size effect on the four point shear behaviour.

In the four point shear test, stress intensification is produced in both the crack tip regions and the stress-intensity factors for mode I and mode II can be expressed respectively as (Fig. 1):

$$K_{\mathrm{I}} = \frac{P}{tb^{1/2}} f_{\mathrm{I}}\left(\frac{l}{b}, \frac{a}{b}, \frac{c}{b}\right), \tag{2a}$$

$$K_{\mathrm{II}} = \frac{P}{tb^{1/2}} f_{\mathrm{II}}\left(\frac{l}{b}, \frac{a}{b}, \frac{c}{b}\right), \tag{2b}$$

where f_{I} and f_{II} are the shape functions.

Most relevant mixed mode fracture criteria can be expressed in the approximate form:

$$K_{\mathrm{I}}^2 + q^2 K_{\mathrm{II}}^2 = K_{\mathrm{IC}}^2 = G_{\mathrm{F}} E, \tag{3}$$

where q is a measure of influence of mode II on crack branching. Equations (2) and (3) provide:

$$\frac{P_{\max}}{tb^{1/2}} = \frac{K_{\mathrm{IC}}}{\sqrt{f_{\mathrm{I}}^2 + q^2 f_{\mathrm{II}}^2}}. \tag{4}$$

If the geometric ratios l/b and a/b are constant, eq. (4) becomes:

$$\frac{P_{\max}}{\sigma_{\mathrm{u}} t\, b} = \frac{s}{F\left(\frac{c}{b}\right)}, \tag{5}$$

where s is the brittleness number[12]:

$$s = \frac{K_{\mathrm{IC}}}{\sigma_{\mathrm{u}} b^{1/2}}. \tag{6}$$

On the other hand, splitting at the centre of the specimen occurs when[7, 12]:

$$\frac{P_{\max}}{\sigma_{\mathrm{u}} t\, b} = \frac{\pi}{2}\left[1 + \left(\frac{c}{b}\right)^2\right]\left(1 + \frac{c}{l}\right). \tag{7}$$

Equations (5) and (7) are in competition by varying the value of the brittleness number and a size-scale transition occurs like that described in Figs 7(a) and (b). The bilinear diagram represents the size-scale transition when the two failure mechanisms are non-interacting. On the other hand, such an interaction is simulated by the cohesive crack model. The curve obtained according to the cohesive crack model, is tangent in the origin to the straight line of eq. (5)[9], while the horizontal line of eq. (7) represents an asymptote for $s \to \infty$. The experimental results in Fig. 7 reproduce the

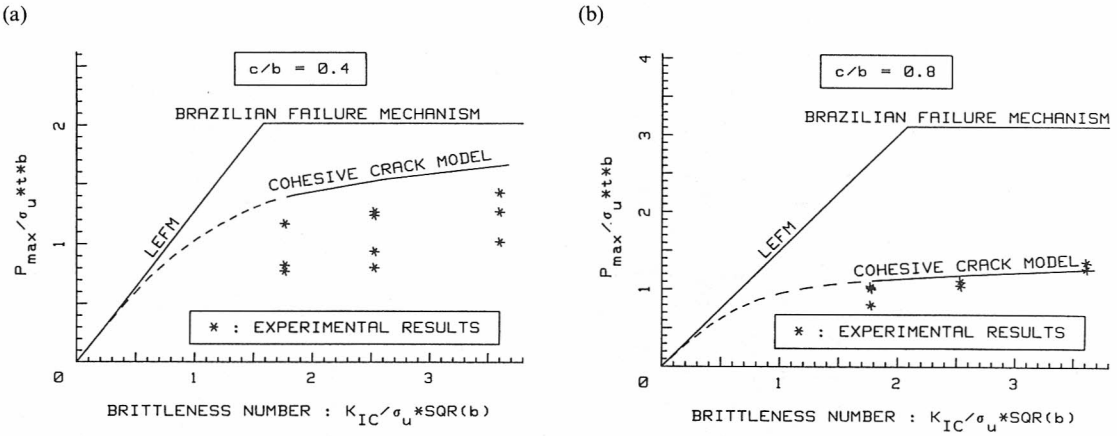

Fig. 7. Size-scale transition from mixed mode LEFM to splitting at the specimen center: (a) $c/b = 0.4$; (b) $c/b = 0.8$.

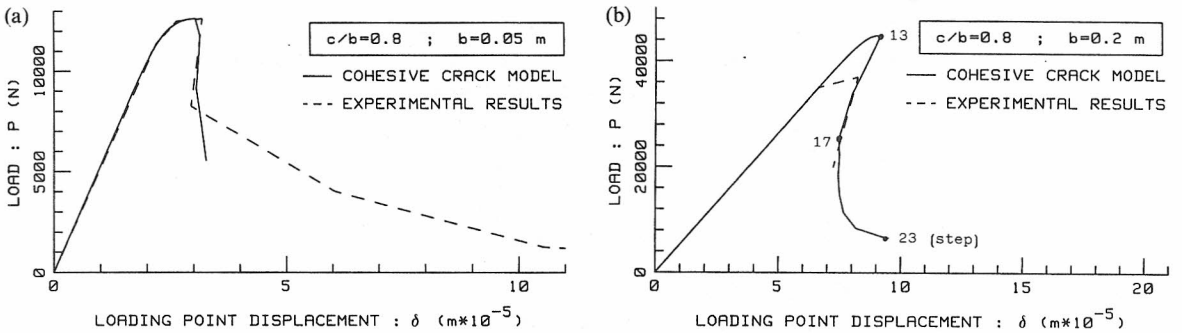

Fig. 8. Experimental load vs deflection curves and numerical cohesive crack simulation, for $c/b = 0.8$: (a) $b = 5$ cm; (b) $b = 20$ cm.

numerical curves with a sufficient accuracy. For the ratio $c/b = 0.4$ (Fig. 7a), the cases explored in the present investigation are closer to the asymptotical condition than they are for $c/b = 0.8$ (Fig. 7b). This means that the splitting failure is favoured by small c/b ratios.

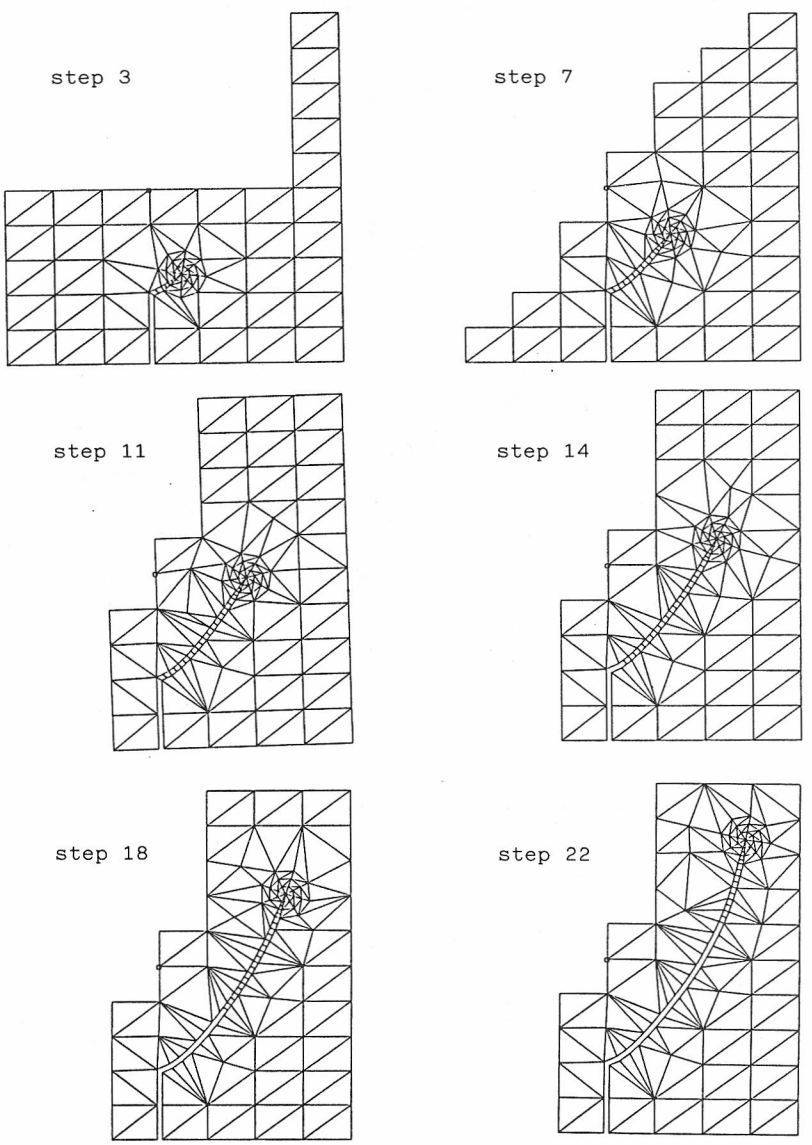

Fig. 9. Finite element remeshing: $c/b = 0.8$; $b = 20$ cm.

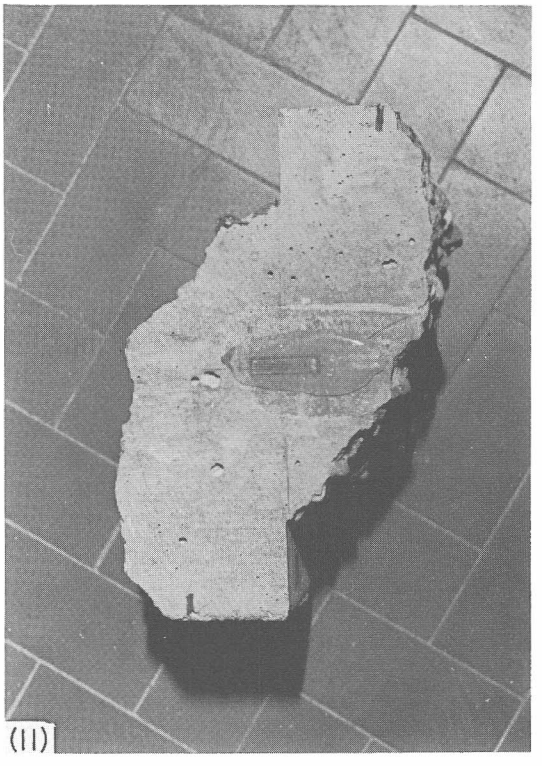

Fig. 11. Experimental trajectories followed by the two symmetrical cracks in the case $c/b = 0.4$, $b = 20$ cm. Two deviations at the beam edges can be observed.

For $c/b = 0.8$, the total load vs loading point deflection diagrams are plotted in Figs 8(a) and (b), in the cases $b = 5$ and 20 cm, respectively. The mixed mode cohesive model (see Section 3) describes both the experimental curves satisfactorily. The size $b = 20$ cm (Fig. 8b) produces snap-back instability in the experimental as well as in the numerical curve. The mechanical properties utilized in the numerical analysis are those reported in Table 1. The area enclosed between numerical curve and deflection axis is approximately equal to the product of mode I fracture energy G_F by total fracture area, and represents the amount of energy dissipated in the localized fracture zone. The amount of energy dissipated by punching at the supports, was deliberately neglected, assuming ascending elastic branches consistent with the elastic modulus of the material (Fig. 8).

It is remarkable that the application of the usual mode I fracture energy G_F only, was able to provide consistent results. It was unnecessary to introduce additional fracture toughness parameters, like, for example, the mode II fracture energy G_F^{II}[8, 11]. As a matter of fact, the mixed mode fracture energy results approximately equal to the mode I fracture energy G_F, each crack growth step being produced by a mode I (or opening) mechanism along the curvilinear trajectory.

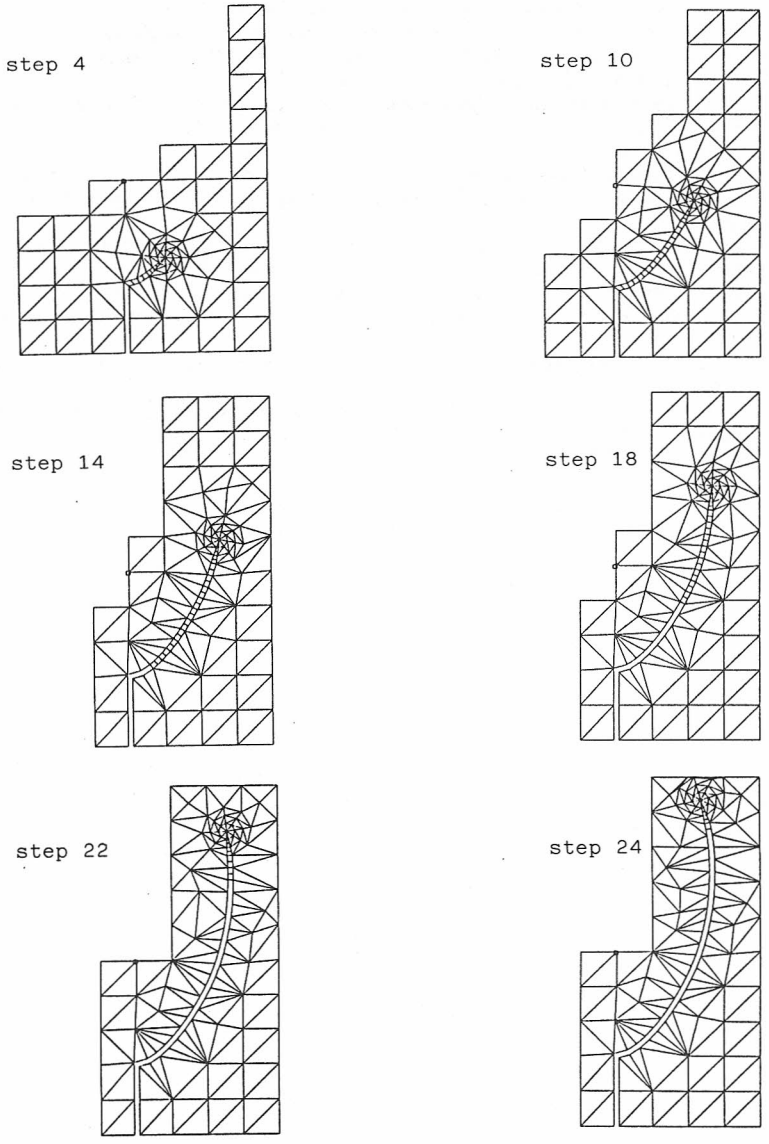

Fig. 10. Finite element remeshing: $c/b = 0.4$; $b = 20$ cm.

The sequence of the finite element meshes utilized for the case $b = 20$ cm, $c/b = 0.8$, is reported in Fig. 9. The trajectory of the finite element rosette reproduces the experimental fracture trajectory accurately. It is remarkable that the real crack (complete disconnection) starts propagating only at the 13th step, when the fictitious crack (cohesive interaction) is beyond one half of the beam depth. On the other hand, at the 22nd step, both fictitious and real crack are close to the upper beam edge. The single steps are indicated also in the diagram of Fig. 8(b).

The sequence of the finite element meshes utilized for the case $b = 20$ cm, $c/b = 0.4$, is reported in Fig. 10. Also in this case, the numerical simulation describes the experimental fracture trajectory very accurately, included the deviations at the beam edges shown in Fig. 11.

Acknowledgements—The financial support of the Department of Public Education (M.P.I.) is gratefully acknowledged.

REFERENCES

[1] G. I. Barenblatt, The formation of equilibrium cracks during brittle fracture: general ideas and hypotheses. Axially-symmetric cracks. *J. appl. Math. Mech.* **23,** 622–636 (1959).
[2] D. S. Dugdale, Yielding of steel sheets containing slits. *J. Mech. Phys. Solids* **8,** 100–104 (1960).
[3] A. Hillerborg, M. Modeer and P. E. Petersson, Analysis of crack formation and crack growth in concrete by means of fracture mechanics and finite elements. *Cem. Concr. Res.* **6,** 773–782 (1976).
[4] A. Carpinteri, Interpretation of the Griffith instability as a bifurcation of the global equilibrium. *NATO Advanced Research Workshop on Application of Fracture Mechanics to Cementitious Composites*, Evanston, Illinois, 4–7 September, 1984 (Edited by S. P. Shah), pp. 284–316. Martinus Nijhoff (1985).
[5] A. Carpinteri and M. Fanelli, Numerical analysis of the catastrophical softening behaviour in brittle structures. *Fourth Int. Conf. on Numerical Methods in Fracture Mechanics*, San Antonio, Texas, 23–27 March, 1987, pp. 369–386. Pineridge Press, Swansea (1987).
[6] A. Carpinteri and S. Valente, Numerical modelling of mixed mode cohesive crack propagation. *Int. Conf. on Computational Engineering Science*, Atlanta, Georgia, 10–14 April, 1988 (Edited by S. N. Atluri and G. Yagawa), pp. 12–VI, Springer (1988).
[7] A. R. Ingraffea and M. J. Panthaki, Analysis of shear fracture tests of concrete beams. *Seminar on Finite Element Analysis of Reinforced Concrete Structures*, Tokyo, Japan, 21–24 May, 1985, pp. 71–91 (1985).
[8] Z. P. Bazănt and P. A. Pfeiffer, Shear fracture tests on concrete. *Mater. Struct.* **19,** 111–121 (1986).
[9] F. Erdogan and G. C. Sih, On the crack extension in plates under plane loading and transverse shear. *J. Basic Engng* **85,** 519–527 (1963).
[10] RILEM Recommendation, Determination of the fracture energy of mortar and concrete by means of three point bend tests on notched beams. *Mater. Struct.* **18,** 287–290 (1985).
[11] J. G. Rots and R. de Borst, Analysis of mixed mode fracture in concrete. *J. Engng Mech.* **113,** 1739–1758 (1987).
[12] A. Carpinteri, Interaction between tensile strength failure and mixed mode crack propagation in concrete. Report to the RILEM Committee 89-FMT (March 1987).

(*Received for publication* 16 *November* 1988)